CrossMark

Relationship Between Solar-Wind Speed and Coronal Magnetic-Field Properties

**Ken'ichi Fujiki[1] · Munetoshi Tokumaru[1] · Tomoya Iju[1] ·
Kazuyuki Hakamada[2] · Masayoshi Kojima[1]**

Abstract We have studied the relationship between the solar-wind speed [V] and the coronal magnetic-field properties (a flux-expansion factor [f] and photospheric magnetic-field strength [B_S]) at all latitudes using data of interplanetary scintillation and solar magnetic field obtained for 24 years from 1986 to 2009. Using a cross-correlation analyses, we verified that V is inversely proportional to f and found that V tends to increase with B_S if f is the same. As a consequence, we find that V has an extremely good linear correlation with B_S/f. However, this linear relation of V and B_S/f cannot be used for predicting the solar-wind velocity without information on the solar-wind mass flux. We discuss why the inverse relation between V and f has been successfully used for solar-wind velocity prediction, even though it does not explicitly include the mass flux and magnetic-field strength, which are important physical parameters for solar-wind acceleration.

1. Introduction

Wang and Sheeley (1990, 1991) showed that the solar-wind velocity [V] correlated inversely with the expansion factor [f] of a magnetic-flux tube in the corona, and this inverse relation has been improved by Arge and Pizzo (2000) for solar-wind prediction as $V = 267.5 + 410/f^{2/5}$ (hereafter the WSA equation). Wang, Hawley, and Sheeley (1996) explained this

✉ K. Fujiki
fujiki@stelab.nagoya-u.ac.jp

[1] Solar-Terrestrial Environment Laboratory, Nagoya University, F3-3(250), Furo-cho, Chikusa, Nagoya 464-8601, Japan

[2] Department of Natural Science and Mathematics, Chubu University, 1200 Matsumoto-cho, Kasugai, Aichi 487-8501, Japan

inverse relation with observational data by the difference of f-dependences of the total-energy flux density at the Sun and the ion flux density at the Sun: although both parameters increase with f, the increase of the flux density is steeper than that of the total-energy flux.

Fisk, Schwadron, and Zurbuchen (1999) and Fisk (2003) proposed the solar-wind acceleration model (hereafter the FSK equation),

$$\frac{V_f^2}{2} = \frac{P_i}{\rho_i u_i} - \frac{GM_\odot}{R_\odot},$$ (1)

where V_f, P_i, $\rho_i u_i$, G, $M_\odot$, and $R_\odot$ are the final solar-wind speed (*e.g.* at 1 AU), the Poynting flux at the coronal base, solar-wind mass flux at the coronal base, the gravitational constant, the solar mass, and the solar radius, respectively. The FSK equation indicates the final solar-wind velocity is determined by two parameters, mass flux released from the loops by reconnection with open-field lines and the Poynting flux at coronal base.

Suzuki and Inutsuka (2005) and Suzuki (2006) introduced the dissipation mechanism of MHD waves through the shock process to the additional acceleration process of the solar wind, and proposed the following equation (hereafter the SZK equation):

$$V_{1\,AU}^2 = 2\left[-\frac{R_\odot^2}{4\pi(\rho v r^2)_{1\,AU}}\frac{B_S}{f}\langle\delta B_\perp \delta v_\perp\rangle_S + \frac{\gamma}{\gamma-1}RT_C - \frac{GM_\odot}{R_\odot}\right],$$ (2)

where R, γ, and B_S are, respectively, the gas constant, ratio of specific heats, and photospheric magnetic-field strength. $-\langle\delta B_\perp \delta v_\perp\rangle_S$ indicates the Poynting flux of the sheared magnetic field, corresponding to the Alfvén wave ($-\langle\delta B_\perp \delta v_\perp\rangle_S > 0$ for an outgoing component). Therefore, the SZK equation is a hybrid of the WSA and the FSK models. These three equations have the following similarities: i) in WSA and SZK equations, V is proportional to $1/f$, ii) in the WSA and SZK equations, the f-dependent term works as an additional acceleration, iii) in the FSK and SZK equations, the Poynting flux is used as acceleration energy, iv) another difference is the B_S-dependence of V; although the SZK equation includes B_S explicitly, the WSA and FSK equations are independent of B_S.

The WSA equation has been widely and successfully used for solar-wind velocity prediction because of its simplicity. However, the physical parameters necessary for the solar-wind acceleration process, such as mass flux and energy, are dropped. In order to elucidate the solar-wind acceleration process, we must make a model which includes all necessary corona physical parameters explicitly, such as the FSK and SZK equations. From this viewpoint, B_S will be one of the key parameters. Wang (2010) explained why the WSA equation can drop B_S and the mass flux: both the mass flux and the energy flux at the Sun tend to increase approximately linearly with increasing B_S, but B_S has no systematic relation with V at the Earth: accordingly, the independence of V on B_S causes no inclusion of the mass flux and the energy flux in the equation. This means that if we found a B_S-V relation, then necessarily B_S-related parameters of the mass flux and the energy flux should be included. First of all, we will verify the WSA equation in Section 3. In Sections 4 and 5 we will examine the B_S-V relation and demonstrate that the SZK equation is the model preferable over the others from the viewpoint of solar-wind physics. In Section 6, however, we will show that the WSA equation works better than the SZK equation for solar-wind prediction, and we will explain the reason why B_S and the mass flux can be eliminated from the SZK equation.

This study was began by Hirano *et al.* (2003) with data obtained from 1995 to 1996. Analyses were made of large-scale coronal holes (CHs), which consist of a polar CH, a distinct equatorial- and mid-latitude CH, and a low-latitude polar CH extension. It was revealed that V and B_S/f have a remarkably high correlation, with a correlation coefficient
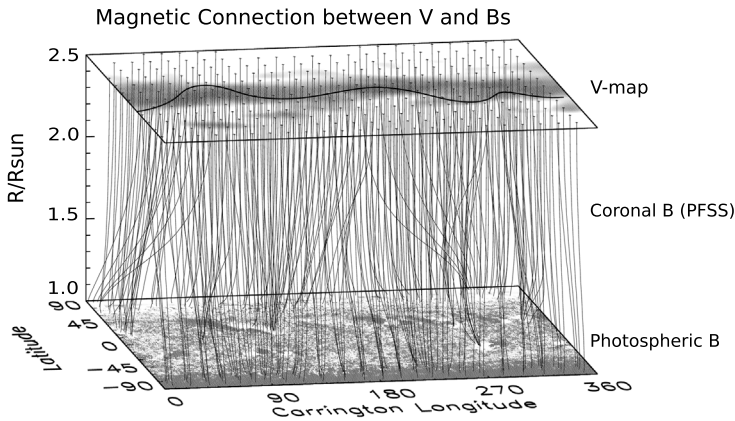
Figure 1 A V-map on the source surface at 2.5 R$_\odot$ is derived by the IPS-tomography method. Potential magnetic-field lines connect the V-map and the photosphere to obtain the flux-expansion factor and B_S.

of 0.88 (Kojima *et al.*, 2004, 2007). Based on their study, here we extend their analyses of data obtained for 24 years from 1986 to 2009, including two solar-minimum phases. In this study, we were particularly interested in comparing the two solar-minimum phases of 1994 – 1996 and 2007 – 2009, because the latter minimum phase showed peculiar aspects compared with the previous one (*e.g.* McComas *et al.*, 2008; Tokumaru *et al.*, 2009; von Steiger and Zurbuchen, 2011; Wang and Sheeley, 2013). Different kinds of CHs, such as a polar CH, a middle-latitude CH, and a CH associated with an active region, have different magnetic-field properties. However, most CHs are at middle and high latitudes where spacecraft cannot approach, with the exception of *Ulysses*. Therefore, in this study, we used tomographic interplanetary scintillation (IPS) measurements, which can derive a solar-wind velocity map over all latitude ranges (Kojima *et al.*, 1998). The data and the analysis method will be explained in Section 2.

2. Data and Analysis

In this study we used three data sets of V, B_S, and f. We used the solar-wind velocities measured at Solar-Terrestrial Environment Laboratory (STEL) using the IPS method because the IPS measurements can observe the solar wind at all latitude ranges in a relatively short time, and the observations cover several solar cycles (Kojima and Kakinuma, 1990). However, the solar-wind velocities that are estimated directly from the IPS measurement involve the line-of-sight integration effect. Therefore, we used the tomographic analysis technique (Kojima *et al.*, 1998), which can deconvolve the line-of-sight integration effects and retrieve the intrinsic solar-wind velocity. Using this technique, we derived velocity distribution maps of latitude and longitude (V-map) on the source surface at 2.5 R$_\odot$ (Figure 1). Since IPS tomographic analysis requires good coverage of line-of-sight projection on the source surface, we used IPS data obtained during three Carrington rotations to derive one V-map. Therefore, each V-map represents the average structure during three Carrington rotations. This data-window of three rotations was shifted by one rotation to derive the map of the next rotation. Thus, we obtained about ten maps each year except for the snowy winter seasons when the IPS observations at STEL were interrupted. The analyses were made for the years from 1986 to 2009 over two solar cycles.
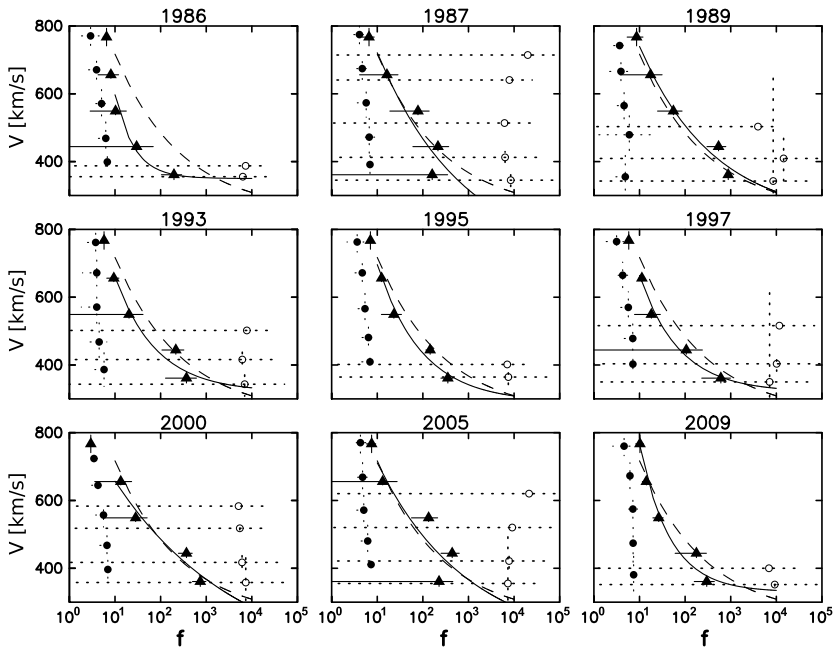
Figure 2 Dependence of velocity on the flux-expansion factor. Triangles are averages of all data in each year. Solid circles are data with weak magnetic-field strength (< 5 G) and small expansion factors (< 100), while open circles are those with strong magnetic-field strength (> 50 G) and a large expansion factor (> 1000). A solid curved line is the best-fit solution for Equation (3), while a dashed line is the average best-fit solution for the 24 years of data from year 1986 to 2009.

In order to obtain magnetic-field properties of B_S and f, we used the solar magnetic-field data observed at the National Solar Observatory/Kitt Peak, and calculated the coronal magnetic-field configuration by the potential-field-source-surface (PFSS) model (Schatten, Wilcox, and Ness, 1969; Altschuler and Newkirk, 1969). The PFSS analysis code was developed by Hakamada and Kojima (1999) and was used for mapping a solar-wind structure obtained by IPS to its counterpart on the photosphere (Ohmi *et al.*, 2001; Kojima *et al.*, 2004). We traced back the velocity map from the source surface to the photosphere along the potential-field line to find the source region of the flow on the photosphere and obtain the photospheric magnetic-field strength B_S (Figure 1). The flux-expansion factor [f] is defined by the ratio between the magnetic-field strength on the photosphere and that on the source surface normalized by $(R_{SS}/R_{\odot})^2$, where R_{SS} is the radius of the source surface. The flux-expansion factors and the photospheric magnetic-field strength were averaged from five solar-wind velocity ranges of $300 – 400$, $400 – 500$, $500 – 600$, $600 – 700$, and > 700 km s^{-1}. Thus, the averages of $f(V_i)$, and $B_S(V_i)$ obtained for each Carrington rotation were averaged again over a year, from which we derived the year-averaged parameters f, B_S, and the ratio between these two parameters [B_S/f] as functions of V.

3. Flux-Expansion Factor [f]

Figure 2 shows the dependence of velocity on the flux-expansion factor for the years 1986, 1987, 1989, 1993, 1995, 1997, 2000, 2005, and 2009. Triangles with solid error bars represent averages of all data in each year. We chose as examples the data of nine years among

Table 1 Average expansion factors for the five solar-wind velocity ranges of $300-400$, $400-500$, $500-600$, $600-700$, and >700 km s^{-1}, respectively. The second row is the average through all years [f_{all}], and the third and fourth rows are averages for three-year periods: $1994-1996$ [f_1] and $2007-2009$ [f_2]. The last row shows the ratio between two periods.

V [km s^{-1}]	$300-400$	$400-500$	$500-600$	$600-700$	>700
f_{all}	373 ± 242	250 ± 151	31 ± 28	11 ± 3	6 ± 2
f_1	221 ± 159	195 ± 79	24 ± 2	12 ± 1	7 ± 0.4
f_2	276 ± 21	167 ± 63	35 ± 11	14 ± 0.4	10 ± 0.5
f_2/f_1	1.25 ± 0.58	0.86 ± 0.65	1.46 ± 0.22	1.17 ± 0.08	1.43 ± 0.05

the 24 years, including the solar-minimum and solar-maximum phases. Solid curved lines represent the best-fit solution for

$$V = V_0 + \alpha/f^{\beta}, \tag{3}$$

while the dashed lines represent the best-fit solution averaged for all data during 24 years given by

$$V = 250 + 932/f^{0.30}. \tag{4}$$

The inverse relation between velocity and the flux-expansion factor was originally found by Wang and Sheeley (1990, 1991), and its inverse equation has been improved by Arge and Pizzo (2000) for solar-wind prediction. The original Wang and Sheeley equation was based upon the empirical correlation between the velocities observed at the Earth and the flux-expansion factor derived with the data measured at the Wilcox Solar Observatory. On the other hand, Arge and Pizzo (2000) propagated the solar-wind predicted on the source surface using Equation (3) to the Earth, and then made iterations changing parameters in the equation until a reasonably good agreement was obtained between *in-situ* observations and predicted velocities at the Earth. Although Equation (4) can be applied for all latitudes, the WSA equation should be applied for the observations near the solar Equator because it was derived by making an iterative comparison with the low-latitude *in-situ* data. The numerators of the second term in Equation (4) and the WSA equation exhibit a two-fold difference. This was caused mainly by the difference in the magnetic-field data, and therefore Equation (4) should be applied to Kitt Peak data, which were measured with a higher spatial resolution than those of the Wilcox Solar Observatory.

Figure 3 shows yearly variations in the expansion factors derived for the five solar-wind velocity ranges of $300-400$, $400-500$, $500-600$, $600-700$, and >700 km s^{-1}. We compared the flux expansions between the last solar minimum ($2007-2009$) and the previous minimum ($1994-1996$) in Table 1. The differences were less than 1σ variances of the all-year averages, but between two minimum phases, there were small but statistically significant differences in medium- and high-velocity winds. In the last solar minimum, f increased 1.1 to 1.4 times, and this increase was similar to that reported by Wang and Sheeley (2013), who compared *Ulysses* polar passes in $1993-1996$ and $2006-2008$, finding an increase of 1.2 times and a decrease in the median wind velocity by 3 % (from 740 km s^{-1}).

In order to compare this $V-f$ correlation with two other correlations of $V-B_{\text{S}}$ and $V-B_{\text{S}}/f$ in the following sections, we selected two kinds of solar wind. One originates from the region with weak magnetic-field strength (< 5 G) and a small expansion factor (< 100) (solid circles with dotted error bars in Figure 2, hereafter referred to SW1), and the other one from the region with strong magnetic-field strength (> 50 G) and a large expansion
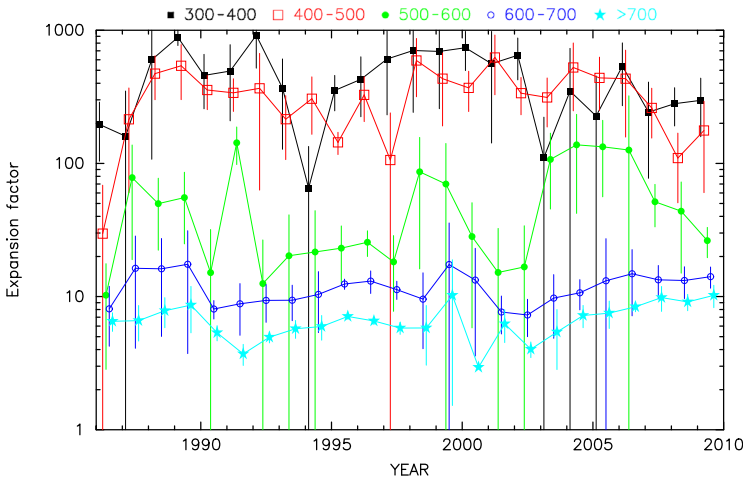
Figure 3 Yearly variation in the expansion factors for the five solar-wind velocity ranges of $300-400$, $400-500$, $500-600$, $600-700$, and >700 km s^{-1}, respectively.

Table 2 Average photospheric magnetic-field strength for the five solar-wind velocity ranges same as Table 1 during three-year periods: $1994-1996$ [B_1] and $2007-2009$ [B_2]. The last row shows the ratio of the average magnetic-field strength between two periods.

V [km s^{-1}]	$300-400$	$400-500$	$500-600$	$600-700$	>700
B_1 [G]	12.5 ± 1.7	11.6 ± 3.5	10.2 ± 1.0	10.3 ± 0.2	10.3 ± 0.4
B_2 [G]	6.9 ± 0.5	7.6 ± 0.6	7.3 ± 0.6	7.5 ± 0.4	8.2 ± 0.6
B_2/B_1	0.6 ± 0.3	0.7 ± 0.5	0.7 ± 0.2	0.7 ± 0.1	0.8 ± 0.1

factor (> 1000) (open circles with dotted error bars, hereafter referred to as SW2). We note in Figure 2 that these data not only deviate substantially from the average group, but also that they are less dependent on f.

4. Photospheric Magnetic-Field Strength [B_S]

Figure 4 shows examples of the dependence of velocity on the photospheric magnetic-field strength for the years 1986, 1987, 1989, 1993, 1995, 1997, 2000, 2005, and 2009. Triangles with solid error bars are averages of all data in each year. An inverse relation between V and B_S exists, but not obviously in the three solar minima (1986, 1995, and 2009). Figure 5 shows yearly variation in the magnetic-field strength derived for the five solar-wind velocity ranges of $300-400$, $400-500$, $500-600$, $600-700$, and >700 km s^{-1}. The average B_S during the three years around the two solar-minimum phases of 1994 to 1996 and 2007 to 2009 are shown in Table 2. In the solar-minimum phase, B_S has a very small range of $10.3-12.5$ G and $6.9-8.2$ G. This is one of the reasons why the inverse relations between V and B_S (triangle) are not obvious in the three solar minima. Comparing the two minimum phases, the field strength of the last minimum phase decreased about 30 % (Table 2) of that of the previous minimum. Wang and Sheeley (2013) also reported a 31 % decrease from 10.6 to 7.3 G in footpoint field strength of the polar wind.
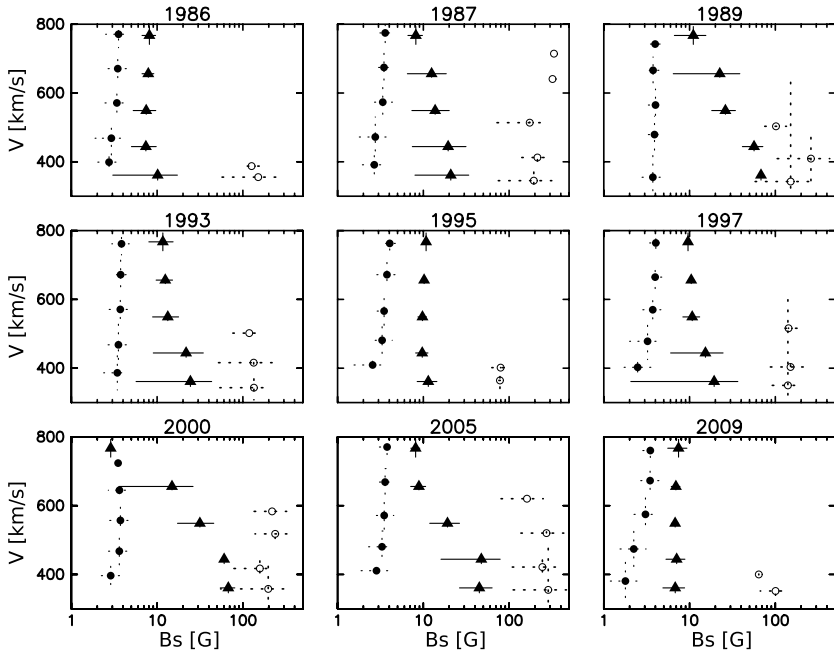
Figure 4 Dependence of velocity on the photospheric magnetic-field strength. Triangles are averages of all data in each year. Solid circles are data with weak magnetic-field strength (< 5 G) and a small expansion factor (< 100), while open circles are data with a strong magnetic-field strength (> 50 G) and a large expansion factor (> 1000).

The FSK equation indicates that the solar-wind velocity at the Earth should have positive dependence on the photospheric-field strength. However, we cannot see this tendency in Figure 4, and furthermore Wang, Hawley, and Sheeley (1996), Wang, Robbrecht, and Sheeley (2009), and Wang and Sheeley (2013) reported that there appears to be almost no systematic relation between them. However, the SZK equation indicates that the additional acceleration term has a positive dependence on B_S. Since this term includes not only B_S but also some other physical parameters such as f and the mass flux, we examined the dependence on B_S, classifying the data by the expansion factor [f]. Data are classified into three expansion factors of $5 - 11$, $11 - 25$, and $25 - 78$. Figure 6 shows as examples three years (1986, 1989, and 1992), which include solar-minimum and -maximum phases. The figures show that velocity increases with B_S when the flux expansion is small, and the dependency becomes less obvious as the flux expansion increases. This behavior can be understood by the first term in Equation (2); as f becomes large, the first term, which includes B_S/f, becomes less effective for determining the final velocity.

In Figure 4 we showed two special kinds of solar wind (solid and open circles). Solid circles are the SW1 with weak magnetic-field strength (< 5 G) and a small expansion factor (< 100), and open circles are SW2 with a strong magnetic-field strength (> 50 G) and a large expansion factor (> 1000). We note that SW1 (solid circle) have a positive relation between V and B_S, unlike the data of the total average (triangles).
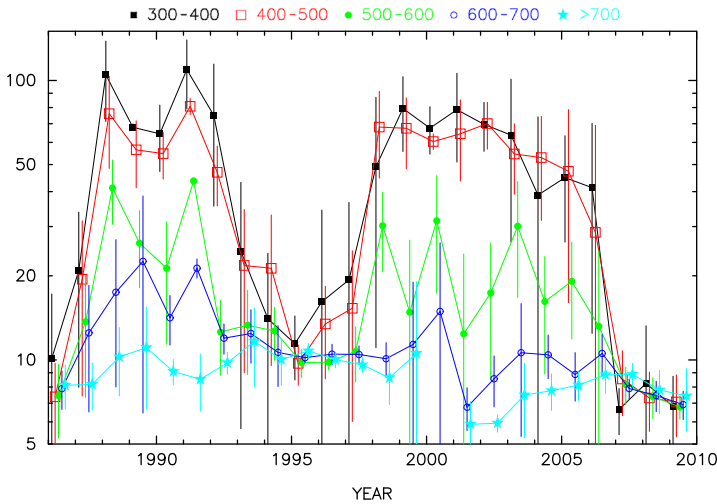
Figure 5 Yearly variation of the magnetic-field strength of photospheric source regions for the five solar-wind velocity ranges same as Figure 3.

5. Ratio of Magnetic Field Strength and Flux-Expansion Factor [B_S/f]

Since the velocity is dependent not only on the inverse of the flux-expansion factor [$1/f$] but also on the photospheric magnetic-field strength [B_S], we here combined these two parameters as B_S/f to examine the relation with velocity. Practically the parameter B_S/f can be replaced by the magnetic field at the source surface [B_{SS}] in the PFSS analysis. Figure 7 shows as examples the dependence of velocity on B_S/f for the years 1986, 1987, 1989, 1993, 1995, 1997, 2000, 2005, and 2009. According to the SZK equation, the correlations are shown for V^2. Solid lines represent the best-fit line for the equation

$$V^2 = V_0^2 + \alpha \frac{B_S}{f}, \tag{5}$$

while dashed ones represent

$$V^2 = 247^2 + 613^2 \frac{B_S}{f}, \tag{6}$$

which was obtained by averaging 24 years of data. Although the best-fit line changes year by year, V^2 had a fairly good linear dependence on B_S/f throughout the 24 years.

In order to see the features of the $V - B_S/f$ correlation as compared with the other two correlations of $V - f$ and $V - B_S$, we note the two special kinds of solar wind of SW1 and SW2 shown by open and closed circles in Figure 7. Although these kinds of solar wind deviated substantially from the major average groups in f (Figure 2) and B_S (Figure 4) correlation diagrams, the SW1 data fit well on the linear relation with B_S/f. However, SW2 does not have an obvious dependence on B_S/f, having a small value of B_S/f.

Figure 8 shows the yearly variation of B_S/f derived for the five solar-wind velocity ranges of $300-400$, $400-500$, $500-600$, $600-700$, and >700 km s^{-1}, and Table 3 compares variations between the two solar-minimum phases. B_S/f in the last minimum phase decreased from that in the previous phase, and high-velocity winds ($600-700$ and >700 km s^{-1}) especially decreased by as much as 50 %. The major percent of this decrease was caused by the 30 % decrease of B_S (Table 2) and the 10 to 40 % increase of f (Table 1).
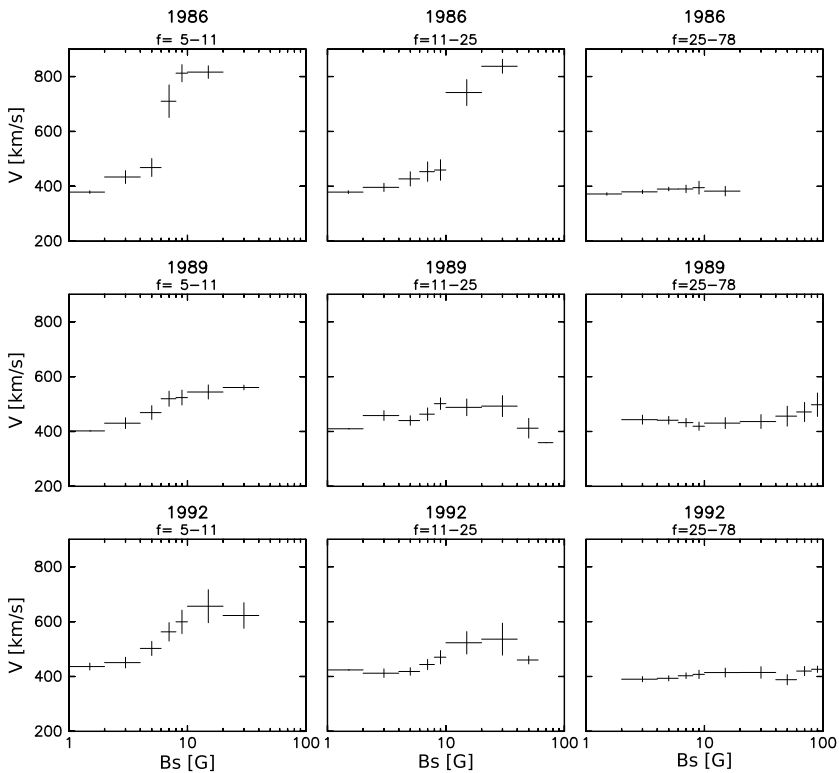
Figure 6 Dependence of velocity on the photospheric magnetic-field strength. Data are classified into three expansion-factor bins, $5-11$, $11-25$, and $25-78$. The three years of 1986, 1989, and 1992 are illustrated.

Table 3 Average B_S/f for the five solar-wind velocity ranges same as Table 1 during three-year periods: $1994-1996$ [$(B_S/f)_1$] and $2007-2009$ [$(B_S/f)_2$]. The last row shows the ratio between two periods.

V [km s^{-1}]	$300-400$	$400-500$	$500-600$	$600-700$	> 700
$(B_S/f)_1$	0.176 ± 0.072	0.297 ± 0.056	0.599 ± 0.142	1.101 ± 0.087	1.778 ± 0.019
$(B_S/f)_2$	0.131 ± 0.027	0.187 ± 0.036	0.383 ± 0.056	0.620 ± 0.055	0.906 ± 0.058
$(B_S/f)_2/(B_S/f)_1$	0.74 ± 0.62	0.63 ± 0.43	0.64 ± 0.44	0.56 ± 0.21	0.51 ± 0.13

6. Discussion

We investigated the relation between the solar-wind velocity and the coronal magnetic parameters from 1986 to 2009. From the cross-correlation analysis, we verified that V has an inverse relation with f (Equation (4)) as reported by Wang and Sheeley (1990, 1991). There are reports that both the mass and the energy-flux densities tend to increase approximately linearly with increasing magnetic-field strength, but there appears to be almost no systematic relation between photospheric magnetic-field strength and the solar-wind velocity at the Earth (Wang, Hawley, and Sheeley, 1996; Wang, Robbrecht, and Sheeley 2009; Wang and Sheeley, 2013). However, we found a different relation between photospheric magnetic-field strength and the solar-wind velocity. Investigating the $V-B_S$ relations for the
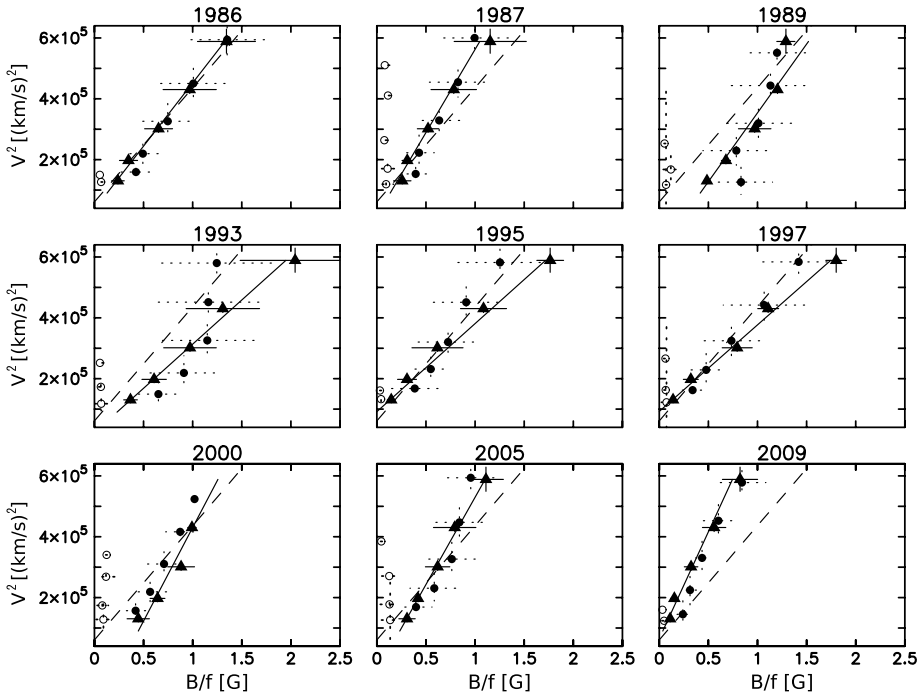
Figure 7 Dependence of velocity on the ratio of photospheric magnetic-field strength and a flux-expansion factor. Triangles are averages of all data in a year. Solid circles are SW1 with weak magnetic-field strength (< 5 G) and a small expansion factor (< 100), and open circles are SW2 with strong magnetic-field strength (> 50 G) and a large expansion factor (> 1000). Solid lines are the best-fit regression lines, while dashed lines are the average for the 24 years of data from 1986 to 2009.

solar wind binned by the flux-expansion factor, we found that the higher-velocity winds flow out of stronger-field regions in each bin. Combining these two relations of $V-f$ and $V-B_{\mathrm{S}}$, we revealed that the B_{S}/f has an extremely good linear correlation with the square of the velocity (Equation (6)). This linear correlation also holds for the solar wind from CHs that have a weak magnetic field and a small expansion factor, although they substantially deviated from the $V-f$ correlation.

We compared Equations (4) and (6), which are better models for making solar-wind predictions through the whole solar cycle. Since these equations were derived from averaging 24 years of data, we examined discrepancies in them from the equations obtained for each year (discrepancies between the dashed line and the solid line in Figures 2 and 7). Figure 9 examines Equation (4). The discrepancies are shown for four different expansion factors of 426, 78, 25, and 11 which give velocities of 400, 500, 600, and 700 km s^{-1} from Equation (4), respectively. The average discrepancies over the 24 years are -11 ± 23, -22 ± 40, -30 ± 48, and -30 ± 48 km s^{-1} at each of the four expansion factors. This means that a prediction over the whole solar cycle can be made accurately using the single equation. In particular, the prediction of low- and medium-velocity solar winds, which are usually observed at the solar Equator, can be made with accuracy better than 50 km s^{-1}.

Figure 10 examines Equation (6). Discrepancies between dashed lines and solid lines in Figure 7 are shown for three different values of B_{S}/f (0.264, 0.503, and 0.796 [G]), which give velocities of 400, 500, and 600 km s^{-1} from Equation (6). Figure 10 indicates that this

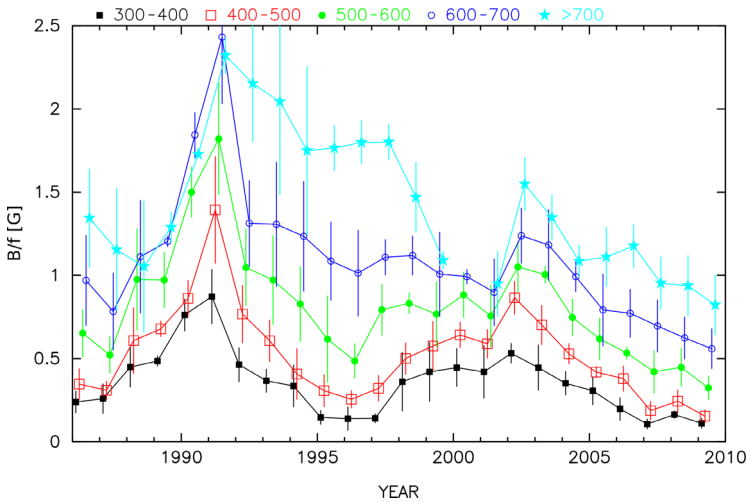**Figure 8** Yearly variation of B_S/f for the five solar-wind velocity ranges same as Figure 3.
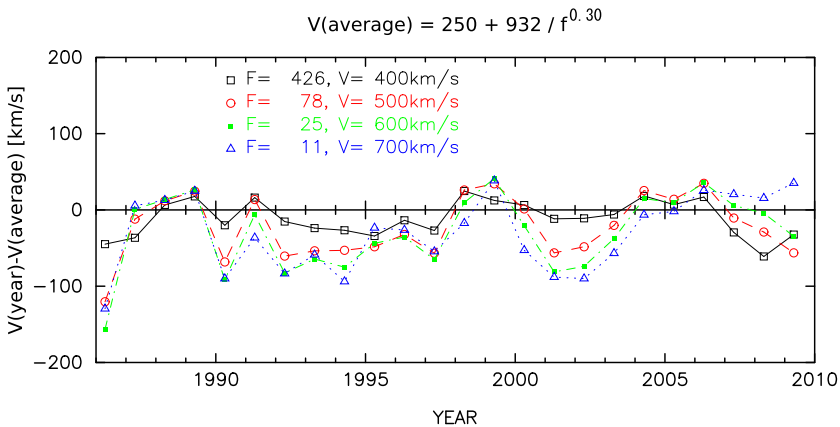

Figure 9 Differences in the best-fit solutions between the solid line and the dotted line in Figure 2. The discrepancies are shown for four different expansion factors of 2663, 489, 160, and 69, which give velocities of 400, 500, 600, and 700 km s^{-1} from Equation (4), respectively.

single equation cannot be applied for solar-wind prediction through the whole solar cycle. This is because not only B_S/f but also the parameter α change significantly from year to year. This result reflects the following two facts: i) the parameter B_S/f, which is exactly the same as the magnetic-field strength on the source surface in this analysis, determines the global magnetic structure in interplanetary space and depends mainly on the solar magnetic dipole moment which changes significantly through solar cycle, and ii) the range of solar-wind velocity hardly changes through the solar cycle.

It has been reported that the polar solar wind decreased in velocity in 2006–2008 compared with that observed in 1993–1996, but the decrease was as small as 3 % (from 763 to 740 km s^{-1}) (McComas *et al.*, 2008; Wang and Sheeley, 2013). On the other hand, the changes of B_S, f, and B_S/f between the two minimum phases were not small. In particular,
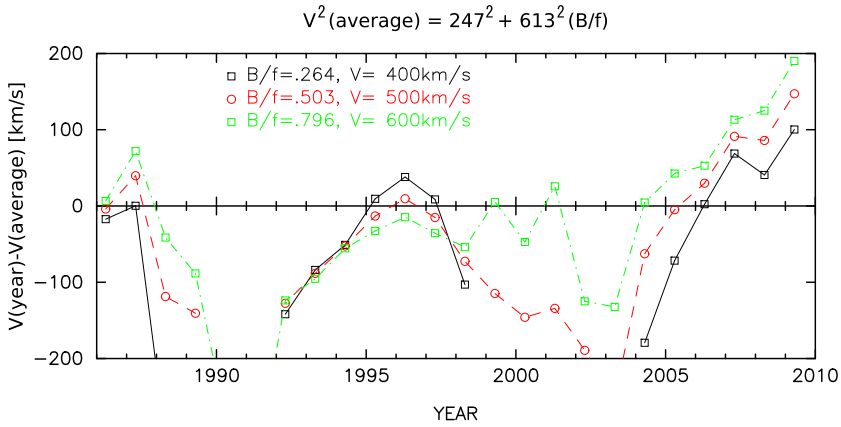
Figure 10 Difference in the best-fit solutions between the solid line and the dotted line in Figure 7. The discrepancies are shown for three values of B_S/f of 0.068, 0.102, and 0.144 G, which give velocities of 400, 500, and 600 km s^{-1} from Equation (6), respectively.
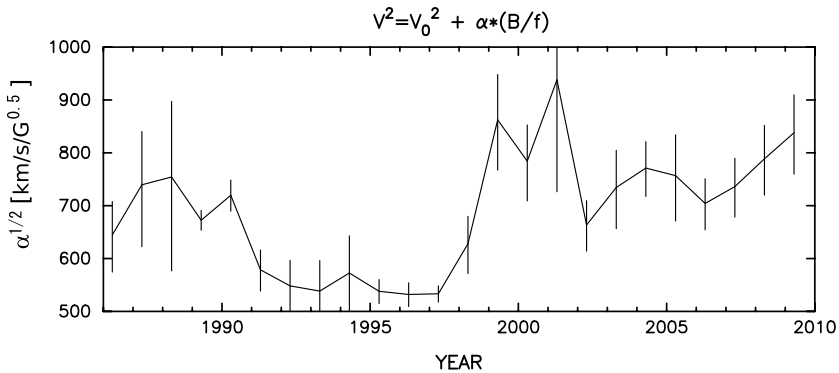

Figure 11 Yearly variation of the gradient [α] of Equation (5).

the change of the parameter α in Equation (5) was as large as 200 % between the two minimum phases (Figure 11 and Table 4). The less significant change of the polar high-velocity wind between two minimum phases can be understood by the second term of Equation (5), $\alpha B_S/f$, which gives additional acceleration to the thermal-driven solar wind. Since α increased 200 % and B_S/f decreased about 50 % (Table 3), the change of the additional acceleration is small.

The square of the first term in Equation (6), V_0^2, corresponds to $2[\gamma/(\gamma - 1)RT_c - (GM_\odot/R_\odot)]$ in the SZK equation. Therefore, $V_0^2/2 + GM_\odot/R_\odot$ is proportional to the coronal temperature [T_c], and the V_0 decrease of 25 % between two minimum phases (Table 4) corresponds to a 6 % decrease of coronal temperature. This is the same freeze-in temperature decrease derived from the ion charge ratio of the solar wind by von Steiger and Zurbuchen (2011).

According to the SZK equation, α varies in proportion to the inverse of the mass flux. Although the solar-wind velocity did not change significantly between the two minimum phases, solar-wind densities provided by NASA/GSFC's Space Physics Data Facility's OM-

Table 4 Comparison of averaged parameters V_0 and α in Equation (5) between two solar-minimum phases. The third column represents averaged B_S/f for $V = 750\ \mathrm{km\,s^{-1}}$. The last row shows the ratio between the two periods.

Period	V_0	α	B_S/f [750 $\mathrm{km\,s^{-1}}$]
1994 – 1996	321 ± 20	$535^2 \pm 57^2$	1.778 ± 0.019
2007 – 2009	237 ± 43	$782^2 \pm 255^2$	0.906 ± 0.058
$\frac{2007-2009}{1994-1996}$	0.74 ± 0.26	2.13 ± 0.05	0.51 ± 0.13

Table 5 Average solar-wind density at 1 AU for the five solar-wind velocity ranges same as Table 1 during three-year periods: 1994 – 1996 [N_1] and 2007 – 2009 [N_2]. The last row shows the ratio between the two periods.

V [$\mathrm{km\,s^{-1}}$]	300 – 400	400 – 500	500 – 600	600 – 700	> 700
N_1 [$\mathrm{cm^{-3}}$]	11.13 ± 6.29	6.70 ± 4.30	4.29 ± 2.17	3.49 ± 1.34	3.19 ± 2.32
N_2 [$\mathrm{cm^{-3}}$]	6.77 ± 4.84	4.11 ± 3.01	2.96 ± 1.74	2.58 ± 0.89	2.01 ± 0.61
N_2/N_1	0.61 ± 3.85	0.61 ± 2.68	0.69 ± 1.55	0.74 ± 1.02	0.63 ± 1.47

NIweb service decreased from 30 to 40 % (Table 5). McComas *et al.* (2008) also reported that the fast solar wind from both large polar CHs was significantly less dense (17 %) than during the previous solar minimum. Therefore, half of the α increase could be attributed to this density decrease. Since α also consists of the Poynting flux from the photosphere [$\langle \delta B_\perp \delta v_\perp \rangle_S$], another half of the α increase may have been caused from an increase of the Poynting flux. From this viewpoint, it is worth noting that Wang and Sheeley (1991) commented that if Alfvén waves were responsible for accelerating the solar wind, and the wave-energy flux is roughly constant, the mean-square wave velocity [$\langle \delta v_0^2 \rangle$] and the field strength [B_S] at the coronal base may be inversely correlated.

Making cross-correlation analyses between the solar-wind data measured by the *Advanced Composition Explorer* (ACE) spacecraft and the photospheric magnetic-field strength, Wang and Sheeley (2013) obtained the following equation between the mass-flux density at the coronal base and the footpoint field strength:

$$n_0 v_0 \approx 8 \times 10^{12}\ \mathrm{cm^{-2}\,s^{-1}}\, B_S\ \mathrm{[G]}, \tag{7}$$

where B_S is a footpoint field strength. Therefore, if we compare the solar-wind streams, which have the same flux-expansion factor, $B_S/n_e v_e$ is a constant value that does not depend on solar activity. In fact, Tables 2 and 5 show that the changes of B_S and $n_e v_e$ between the two minimum phases are of the same amount: 30 %. Consequently, the mass flux and the magnetic-field strength disappear from the additional acceleration term in the SZK equation, becoming const. $\times \langle \delta B_\perp \delta v_\perp \rangle_S / f$, which is similar to the WSA equation except for the Poynting flux. This equation can be made equivalent to the WSA equation, by making the Poynting flux less dependent on the solar activity. However, we discussed above that the Poynting vector has to be about 1.4 times larger in the last minimum phase to make the additional acceleration term in the SZK equation less sensitive to solar activity. This contradiction must be investigated in a further study.

7. Conclusions

We investigated the relation between the solar-wind velocity and the coronal magnetic parameters by comparing the WSA and SZK equations. We verified that V is inversely proportional to f and found that V tends to increase with B_S if f is the same. Consequently, we revealed that V has an extremely good linear correlation with B_S/f as indicated by the SZK equation. However, we should note that the SZK equation (the $V - B_S/f$ relation) cannot be used for solar-wind prediction through the whole solar cycle. The slope of its linear relation changes year by year largely because it explicitly includes a mass flux. On the other hand, the WSA equation [$V - f$ relation] is a good prediction model, which can be used through the whole solar cycle, although it includes neither the mass flux nor B_S, which play important physical roles for the additional acceleration of the solar wind. This is because the mass flux and magnetic-field strength can be canceled in the SZK equation using their linear relation.

The slope of the linear $V - B_S/f$ relation shows a solar-cycle variation. We focused especially on the comparison between the two solar-minimum phases: $1994 - 1996$ and $2007 - 2009$. Consequently we found that the slope is two times larger in the very quiet solar minimum ($2007 - 2009$) in comparison with that in $1994 - 1996$. This difference in solar-minimum phases is probably explained by a long-term variation of the solar-cycle activity. However, the slope also tends to increase during solar active phases, which was not discussed in this article; we will extend this examination including the whole solar cycle in a further study.

References

Altschuler, M.D., Newkirk, G.: 1969, Magnetic fields and the structure of the solar corona. I: methods of calculating coronal fields. *Solar Phys.* **9**, 131. DOI.

Arge, C.N., Pizzo, V.J.: 2000, Improvement in the prediction of solar wind conditions using near-real time solar magnetic field updates. *J. Geophys. Res.* **105**, 10465. DOI.

Fisk, L.A.: 2003, Acceleration of the solar wind as a result of the reconnection of open magnetic flux with coronal loops. *J. Geophys. Res.* **108**, 1157. DOI.

Fisk, L.A., Schwadron, N.A., Zurbuchen, T.H.: 1999, Acceleration of the fast solar wind by the emergence of new magnetic flux. *J. Geophys. Res.* **104**, 19765. DOI.

Hakamada, K., Kojima, M.: 1999, Solar wind speed and expansion rate of the coronal magnetic field during Carrington Rotation 1909. *Solar Phys.* **187**, 115. DOI.

Hirano, M., Kojima, M., Tokumaru, M., Fujiki, K., Ohmi, T., Yamashita, M., Hakamada, K., Hayashi, K.: 2003, The relation between the solar wind velocity and the magnetic conditions of coronal holes. In: *AGU Fall Meeting Abstracts*. B164.

Kojima, M., Kakinuma, T.: 1990, Solar cycle dependence of global distribution of solar wind speed. *Space Sci. Rev.* **53**, 173. DOI.

Kojima, M., Tokumaru, M., Watanabe, H., Yokobe, A., Asai, K., Jackson, B.V., Hick, P.L.: 1998, Heliospheric tomography using interplanetary scintillation observations 2. Latitude and heliocentric distance dependence of solar wind structure at $0.1 - 1$ AU. *J. Geophys. Res.* **103**, 1981. DOI.

Kojima, M., Fujiki, K., Hirano, M., Tokumaru, M., Ohmi, T., Hakamada, K.: 2004, Solar wind properties from IPS observations. In: Poletto, G., Suess, S.T. (eds.) *The Sun and the Heliosphere as an Integrated System*, *Astrophys. Space Science Lib.* **317**, Springer, Heidelberg 147.

Kojima, M., Tokumaru, M., Fujiki, K., Itoh, H., Murakami, T., Hakamada, K.: 2007, What coronal parameters determine solar wind speed? In: Shibata, K., Nagata, S., Sakurai, T. (eds.) *New Solar Physics with Solar-B Mission* **369**, Astron. Soc. Pacific, San Francisco 549.

McComas, D.J., Ebert, R.W., Elliott, H.A., Goldstein, B.E., Gosling, J.T., Schwadron, N.A., Skoug, R.M.: 2008, Weaker solar wind from the polar coronal holes and the whole Sun. *Geophys. Res. Lett.* **35**, 18103. DOI.

Ohmi, T., Kojima, M., Yokobe, A., Tokumaru, M., Fujiki, K., Hakamada, K.: 2001, Polar low-speed solar wind at the solar activity maximum. *J. Geophys. Res.* **106**, 24923. DOI.

Schatten, K.H., Wilcox, J.M., Ness, N.F.: 1969, A model of interplanetary and coronal magnetic fields. *Solar Phys.* **6**, 442. DOI.

Suzuki, T.K.: 2006, Forecasting solar wind speeds. *Astrophys. J. Lett.* **640**, L75. DOI.

Suzuki, T.K., Inutsuka, S.-i.: 2005, Making the corona and the fast solar wind: a self-consistent simulation for the low-frequency Alfvén waves from the photosphere to 0.3 AU. *Astrophys. J. Lett.* **632**, L49. DOI.

Tokumaru, M., Kojima, M., Fujiki, K., Hayashi, K.: 2009, Non-dipolar solar wind structure observed in the cycle 23/24 minimum. *Geophys. Res. Lett.* **36**, 9101. DOI.

von Steiger, R., Zurbuchen, T.H.: 2011, Polar coronal holes during the past solar cycle: Ulysses observations. *J. Geophys. Res.* **116**, 1105. DOI.

Wang, Y.-M.: 2010, On the relative constancy of the solar wind mass flux at 1 AU. *Astrophys. J. Lett.* **715**, L121. DOI.

Wang, Y.-M., Hawley, S.H., Sheeley, N.R. Jr.: 1996, The magnetic nature of coronal holes. *Science* **271**, 464. DOI.

Wang, Y.-M., Robbrecht, E., Sheeley, N.R. Jr.: 2009, on the weakening of the polar magnetic fields during solar cycle 23. *Astrophys. J.* **707**, 1372. DOI.

Wang, Y.-M., Sheeley, N.R. Jr.: 1990, Solar wind speed and coronal flux-tube expansion. *Astrophys. J.* **355**, 726. DOI.

Wang, Y.-M., Sheeley, N.R. Jr.: 1991, Why fast solar wind originates from slowly expanding coronal flux tubes. *Astrophys. J. Lett.* **372**, L45. DOI.

Wang, Y.-M., Sheeley, N.R. Jr.: 2013, The solar wind and interplanetary field during very low amplitude sunspot cycles. *Astrophys. J.* **764**, 90. DOI.